CHAOS SUPPRESSION IN PERMANENT MAGNET LINEAR SYNCHRONOUS MOTOR DRIVES USING ADAPTIVE TERMINAL SLIDING MODE CONTROL

Le Thi Thuy Ngan[1], Nguyen Thanh Tung[2], Nguyen Trung Thanh[1], Luu Thi Hue[3], Nguyen Hong Quang[1,*]

DOI: https://doi.org/10.57001/huih5804.2026.105

ABSTRACT

Permanent-magnet linear synchronous motors (PMLSMs) may exhibit Lorenz-type chaos when the load-related parameter exceeds a critical threshold determined from the Hopf structure of the normalized equivalent system. Such behavior leads to irregular oscillations in speed and current, degrades positioning accuracy, and complicates practical operation under uncertain disturbances. This paper develops a chaos detection and suppression framework for a third-order PMLSM-Lorenz system based on adaptive terminal sliding mode control. A cascade sliding structure is constructed to match the system dynamics, while feedback linearization is used to cancel the dominant chaos-inducing term. A terminal sliding component guarantees finite-time convergence, and a dead-zone adaptive gain law updates the switching gain online without requiring prior knowledge of the disturbance bound. The analysis establishes an explicit finite-time stability condition through a Lyapunov argument. Simulation results show that the proposed controller detects the onset of chaos and rapidly drives the system from the chaotic regime to the origin with a convergence time well below the theoretical bound. The method also remains robust under bounded disturbances, reduces gain demand relative to fixed-gain sliding mode control, and achieves improved overall control performance.

Keywords: *PMLSM, Chaos suppression, ATSM, finite-time convergence, Lorenz model.*

[1]Thai Nguyen University of Technology, Vietnam

[2]Thai Nguyen University of Information and Communication Technology, Vietnam

[3]Electric Power University, Vietnam

[*]Email: quang.nguyenhong@tnut.edu.vn

Received: 10/3/2026

Revised: 14/4/2026

Accepted: 29/5/2026

1. INTRODUCTION

Permanent-magnet linear synchronous motors (PMLSMs) are widely used in high-precision positioning systems because of their high force density and fast dynamic response. However, once the operating parameters cross certain critical thresholds, a PMLSM may exhibit chaotic behavior, manifested as unpredictable force and speed oscillations that destabilize the system and severely degrade positioning accuracy. Studies on chaos have shown that the onset of chaos can be identified through the Hopf analysis of the corresponding Lorenz-equivalent system. A wide range of control strategies has therefore been proposed to suppress chaos in electromechanical systems. An adaptive accelerated backstepping controller combined with a type-2 fuzzy neural network (T2-FNN) has been applied to PMSM chaos [1]. Prescribed-time control has been proposed for a four-dimensional PMSM [2]. The equivalent-input-disturbance (EID) approach has also been used to suppress chaos in PMSMs [3]. Although these methods have produced promising results, they generally require detailed model information or prior knowledge of the disturbance structure, which limits their applicability when the disturbance is unstructured or poorly characterized.

Sliding mode control (SMC) has been extensively studied for nonlinear systems because of its inherent robustness to disturbances and parameter uncertainties [4]. Numerous studies have applied SMC to PMSMs and PMLSMs, including fast higher-order nonsingular terminal sliding mode control (NTSMC) combined with a dual-disturbance observer for PMLSMs [5], and sensorless PMSM control based on a fuzzy sliding mode observer [6].

Fuzzy sliding mode control for PMSMs under uncertain disturbances has also been investigated [7], and sliding mode observers for sensorless PMSM speed estimation have likewise been developed [8]. However, classical fixed-gain SMC still suffers from two fundamental drawbacks: (i) the switching gain must be chosen no smaller than the upper bound of the disturbance, which leads to conservative design and induces chattering; and (ii) convergence is only asymptotic, with no explicit finite-time guarantee.

To overcome the slow-convergence limitation, many terminal sliding mode control (TSMC) and higher-order sliding mode variants have been developed, including linear SMC for Hall-sensor-based PMLSMs [9], robust second-order NTSMC for PMLSMs [10], adaptive integral second-order NTSMC for PMLSMs [11], adaptive super-twisting-based fast nonsingular TSMC for PMLSMs [12], finite-time variable-gain fractional-order TSMC for PMLSMs [13], adaptive continuous fast TSMC combined with a super-twisting observer for PMSMs [14], and model-free SMC with dynamic gains based on time-delay estimation for PMLSMs [15]. RBF-neural-network-based adaptive SMC for MIMO systems has also been reported [16]. Most of these methods, however, still require prior knowledge of the disturbance bound or have not been developed for systems exhibiting Lorenz-type chaotic dynamics.

This leads to a clear research gap: a method is still needed that can both detect chaos and simultaneously guarantee (i) finite-time convergence with an explicit time bound, (ii) no prior knowledge of the disturbance bound, and (iii) reduced chattering relative to fixed-gain SMC, for PMLSMs exhibiting Lorenz-type chaos.

In this paper, chaos is detected when the system parameters exceed the threshold derived from the analysis of the Lorenz-equivalent PMLSM model; at the instant chaos is detected, an adaptive terminal sliding mode (ATSM) controller formulated within the framework of [17] is activated immediately. By using an adaptive gain law with a dead zone, the proposed controller satisfies all three requirements above. The main contributions of this paper are as follows. (1) A chaos-detection mechanism is established from the condition inferred through analysis of the Lorenz-equivalent PMLSM system, and the ATSM controller in the framework of [17] is triggered immediately, using a cascade sliding-surface structure tailored to the third-order state equations of the PMLSM-Lorenz model. (2) It is proved, using the Bhat-Bernstein theorem and Lyapunov stability analysis, that the ATSM controller drives the system from the Lorenz-chaotic regime to the stable origin in finite time; an explicit upper bound on the escape time from chaos is derived from the initial conditions and verified numerically. (3) The chaos-suppression performance is assessed comprehensively in quantitative terms by examining robustness when the chaotic system is subjected to bounded but unknown disturbances, analyzing the sensitivity of the detection threshold and the chaos-suppression rate to model parameters, and comparing the proposed method with fixed-gain SMC on the same chaotic plant.

2. MATERIALS AND METHODS

2.1. PMLSM in Lorenz-equivalent form

The PMLSM in the dq frame is modeled as a third-order electromechanical system [5], [8]. After normalization by $t_e = L/R_s$, it becomes a Lorenz-equivalent model [1-3]. The equations in (1) define $x_1 = \omega_e L/R_s$ (normalized speed), x_2 (normalized q-axis current), x_3 (normalized d-axis current), with inputs u_1, u_2 and disturbance $d(t)$ satisfying $|\, d(t) \,| \leq D$, $D > 0$, σ, β, and $\rho(t)$ are the Lorenz-type parameters defined in (2).

$$\begin{aligned} \dot{x}_1 &= \sigma(x_2 - x_1); \\ \dot{x}_2 &= \rho(t)x_1 - x_2 - x_1x_3 + u_1 + d(t); \\ \dot{x}_3 &= x_1x_2 - \beta x_3 + u_2 + d(t) \end{aligned} \tag{1}$$

$$\sigma = \frac{R_s}{L}; \beta = \frac{B}{m}\frac{L}{R_s}; \rho = \frac{3\pi^2\psi_f^2}{2m\tau_p^2R_s^2} - \frac{R_s}{L} \tag{2}$$

The mapping to Lorenz parameters follows (2), where $R_s\,[\Omega]$, $L\,[H]$, $B\,[N \cdot s \cdot m^{-1}]$, $m\,[kg]$, $\psi_f\,[Wb]$, $\tau_p\,[m]$ denote stator resistance, inductance, viscous friction, mover mass, PM flux, and pole pitch.

The corresponding vector-matrix form can be compactly written as equations (3) and (4):

$$\begin{aligned} &\dot{x} = A(\rho)x + \Phi(x) + Bu + Ed(t); \\ &x = [x_1 \quad x_2 \quad x_3]^T; u = [u_1 \quad u_2]^T \end{aligned} \tag{3}$$

$$\begin{aligned} A(\rho) &= \begin{bmatrix} -\sigma & \sigma & 0 \\ \rho(t) & -1 & 0 \\ 0 & 0 & -\beta \end{bmatrix}; \\ \Phi(x) &= \begin{bmatrix} 0 \\ -x_1x_3 \\ x_1x_2 \end{bmatrix}; B = \begin{bmatrix} 0 & 0 \\ 1 & 0 \\ 0 & 1 \end{bmatrix}; E = \begin{bmatrix} 0 \\ 1 \\ 1 \end{bmatrix} \end{aligned} \tag{4}$$

The equilibrium points of the uncontrolled autonomous system $(u_1 = u_2 = 0, d = 0)$ are determined by (5):

$$\begin{aligned} &O = (0,0,0); \\ &C_\pm = \left(\pm\sqrt{\beta(\rho-1)}, \pm\sqrt{\beta(\rho-1)}, \rho-1\right); \rho > 1 \end{aligned} \tag{5}$$

2.2. Chaos onset condition and the two-phase scenario

The stable-chaotic transition follows from linearization at $C_{\pm}$ and the Hopf condition of the Lorenz system [1-3], the Jacobian at $C_{\pm}$ is given by (6):

$$J(C_{\pm}) = \begin{bmatrix} -\sigma & \sigma & 0 \\ 1 & -1 & -x_1^* \\ x_2^* & x_1^* & -\beta \end{bmatrix}; \quad x_1^* = x_2^* = \pm\sqrt{\beta(\rho-1)} \tag{6}$$

The characteristic polynomial of $J(C_{\pm})$ is given by (7), a necessary Hopf condition is (8).

$$\lambda^3 + (\sigma+\beta+1)\lambda^2 + \beta(\sigma+\rho)\lambda + 2\sigma\beta(\rho-1) = 0 \tag{7}$$

$$\sigma > \beta + 1 \tag{8}$$

The critical Hopf threshold is defined by the Routh–Hurwitz boundary (9), so chaos detection reduces to condition (10). Let $\rho(t) = \rho_1$ for $t < t_s$ and $\rho(t) = \rho_2$for $t \geq t_s$ as in (11). This two phase law is a numerical construct to contrast regimes within one simulation. For $t < t_s$, $\rho_1 < \rho_c \Rightarrow$ (9) holds and the system remains stable. For $t \geq t_s$, $\rho_2 > \rho_c \Rightarrow$(10) holds and the system evolves into the chaotic regime.

$$\rho_c = \frac{\sigma(\sigma+\beta+3)}{\sigma-\beta-1} \tag{9}$$

$$\rho(t) > \rho_c \tag{10}$$

$$\rho(t) = \begin{cases} \rho_1 & 0 \leq t < t_s; \rho_1 < \rho_c \\ \rho_2(t) & t \geq t_s; \rho_2(t) > \rho_c \end{cases} \tag{11}$$

The initial state and neighboring equilibrium in phase one are given by (12):

$$x(0) = x_0;\ C_+ = \begin{bmatrix} \sqrt{\beta(\rho_1-1)} \\ \sqrt{\beta(\rho_1-1)} \\ \rho_1 - 1 \end{bmatrix} \tag{12}$$

2.3. ATSM controller design

Since linear PMLSM and rotary PMSM share the normalized Lorenz form (1), ATSM in [17] applies directly, once (10) is detected at $t = t_s$, the goal is $x(t) \to 0$ in finite time, and the cascade sliding surface is given by (13):

$$s_1 = x_1; s_2 = x_2 - \phi; s_3 = x_3 \tag{13}$$

To replace $\mathrm{sgn}(\cdot)$ and soften the control, the boundary-layer saturation function is introduced as (14) [4, 17].

$$\mathrm{sat}\left(\frac{s}{\phi_{bl}}\right) = \begin{cases} \mathrm{sgn}(s), & |\, s\,| > \phi_{bl}, \\ \dfrac{s}{\phi_{bl}}, & |\, s\,| \leq \phi_{bl}, \end{cases} \phi_{bl} > 0 \tag{14}$$

The inner-loop virtual control for x_1 is designed by the terminal law (15), where $k_1 > 0$, $c_1 > 0$, $q \in (0,1)$, and L_1 is the adaptive switching gain.

$$\phi = \frac{1}{\sigma}\begin{bmatrix} -k_1 s_1 - c_1\,\mathrm{sat}\left(\dfrac{s_1}{\phi_{bl}}\right) |\, s_1\,|^q \\ -L_1 \mathrm{sat}\left(\dfrac{s_1}{\phi_{bl}}\right) \end{bmatrix} \tag{15}$$

The nonlinear terms that induce chaotic behavior are separated as (16):

$$f_2(x) = \rho(t)x_1 - x_2 - x_1x_3, \quad f_3(x) = x_1x_2 - \beta x_3 \tag{16}$$

The two-channel control laws are given by (17a) and (17b). In (17), $-f_2(x)$ and $-f_3(x)$ realize local feedback linearization, and $-\rho(t)x_1 \subset -f_2(x)$ cancels the dominant chaotic excitation in (1). Since the disturbance bound D is unknown, the adaptive gains follow the dead-zone laws (18) and (19), where $\lambda_i > 0$ and $d_z > 0$ [17].

$$u_1 = -f_2(x) - k_2 s_2 - c_2\,\mathrm{sat}\left(\frac{s_2}{\phi_{bl}}\right) |\, s_2\,|^q - L_2 \mathrm{sat}\left(\frac{s_2}{\phi_{bl}}\right) \tag{17a}$$

$$u_2 = -f_3(x) - k_3 s_3 - c_3\,\mathrm{sat}\left(\frac{s_3}{\phi_{bl}}\right) |\, s_3\,|^q - L_3 \mathrm{sat}\left(\frac{s_3}{\phi_{bl}}\right) \tag{17b}$$

$$\dot{L}_i = \lambda_i \max\{|\, s_i\,| - d_z, 0\};\ i = 1,2,3 \tag{18}$$

$$(t_s) = L_0;\ L = \begin{bmatrix} L_1 \\ L_2 \\ L_3 \end{bmatrix} \tag{19}$$

2.4. Finite-Time Convergence Analysis

The closed-loop stability of (1) and (13)-(19) is analyzed by Lyapunov theory and the Bhat–Bernstein finite-time theorem [17], with $\tilde{L}_i = L_i - L_i^{\star}$ and $L_i^{\star} > D$, the augmented Lyapunov function is given by (20).

$$V(s, \tilde{L}) = \frac{1}{2}\sum_{i=1}^{3} s_i^2 + \frac{1}{2}\sum_{i=1}^{3} \frac{\tilde{L}_i^2}{\lambda_i} \tag{20}$$

Along the closed-loop trajectories, substituting (15), (17), and (18) into (20), grouping terms, and using $|\, d(t)\,| \leq D$ yields the dissipation inequality (21). Since $\max\{|\, s_i\,| - d_z, 0\} \leq |\, s_i\,|$, (21) implies (22):

$$\dot{V} \leq -\sum_{i=1}^{3} k_i\, s_i^2 - \sum_{i=1}^{3} c_i\, |\, s_i\,|^{1+q} - \sum_{i=1}^{3} (L_i^{\star} - D)\, |\, s_i\,| + \sum_{i=1}^{3} \tilde{L}_i\, (max\{|\, s_i\,| - d_z, 0\} - |\, s_i\,|) \tag{21}$$

$$\dot{V} \le -\sum_{i=1}^{3} c_i \mid s_i \mid^{1+q} \le -c_{\min}(2V)^{\frac{1+q}{2}}; \quad (22)$$

$$c_{\min} = \min\{c_1, c_2, c_3\} > 0$$

Unlike linear SMC, which gives only asymptotic convergence [4], (22) guarantees finite-time convergence; integrating it via Bhat-Bernstein [17] yields the time bound (23). Equivalently, the trajectory leaves the chaotic region and reaches O no later than (24), where $T^{\star}$ is the explicit upper bound from (23), this is a quantitative advantage over earlier PMLSM TSMC methods [12-15].

$$t_{\text{conv}} - t_s \le \frac{\| s(t_s^+) \|_2^{1-q}}{c_{\min}(1-q)} \quad (23)$$

$$t_{\text{conv}} \le t_s + T^{\star} \quad (24)$$

3. RESULTS AND DISCUSSION

To assess robustness, suppression speed, and parameter sensitivity, the disturbed closed-loop system is simulated over T_f and compared with fixed-gain SMC [4, 8]. The integration rule and disturbance profile are given by (25), where $\Delta t, T_f, A_d$, and ω_d denote the time step, final time, disturbance amplitude, and disturbance frequency.

$$\text{RK4}; \Delta t > 0, t \in [0, T_f]; \quad d(t) = A_d \sin(\omega_d t); t \ge t_s \quad (25)$$

The sensitivity study is conducted over a family of perturbed Lorenz parameters collected in the set (26), where δ_σ, δ_β, and δ_ρ denote bounded relative perturbations.

$$\mathcal{S} = \{(\sigma, \beta, \rho_{\text{amp}}) | \sigma = (1+\delta_\sigma)\bar{\sigma}; \beta = (1+\delta_\beta)\bar{\beta}; \rho_{\text{amp}} = (1+\delta_\rho)\bar{\rho}_{\text{amp}}\} \quad (26)$$

The fixed-gain SMC benchmark uses the sliding surface in (13), removes $| s_i |^q$, and replaces adaptive gains with constants as in (27), with $L^{fix} = \begin{bmatrix} L_1^{fix} & L_2^{fix} & L_3^{fix} \end{bmatrix}^T$.

$$\mathcal{S}u_i^{\text{fix}} = -\hat{f}_i(x) - k_i s_i - L_i^{\text{fix}} \text{sat}\left(\frac{s_i}{\phi_{bl}}\right), \quad i = 1,2,3 \quad (27)$$

The performance indices are normalized into the four quantities in (28):

$$J_{\text{esc}} = t_{\text{esc}} - t_s; \; J_x = \int_{t_s}^{T_f} \| x(t) \|_2^2 \, dt;$$

$$J_u = \int_{t_s}^{T_f} \| u(t) \|_2^2 \, dt; \quad (28)$$

$$J_{\text{chat}} = \sum_{k=k_s}^{N-1} \frac{\| u_{k+1} - u_k \|_2^2}{\Delta t}$$

If a compact sensitivity measure is needed, the parametric sensitivity coefficient can be expressed as in (29):

$$S_p = \frac{\Delta J_{\text{esc}}/J_{\text{esc}}}{\Delta p/p}, p \in \{\sigma, \beta, \rho_{\text{amp}}\} \quad (29)$$

Under this formulation, the comparison between ATSM and fixed-gain SMC reduces to three principal axes: escape time from chaos, control effort, and chattering level.

Figure 1 compares the 3D phase portraits of the PMLSM in Phase 2 for the uncontrolled case and ATSM, using the same $x(t_s) = [3.10, 3.17, 8.93]^{\top}$ and $\rho(t) = 28 + 3\sin(3t) > \rho_c = 14.93$.

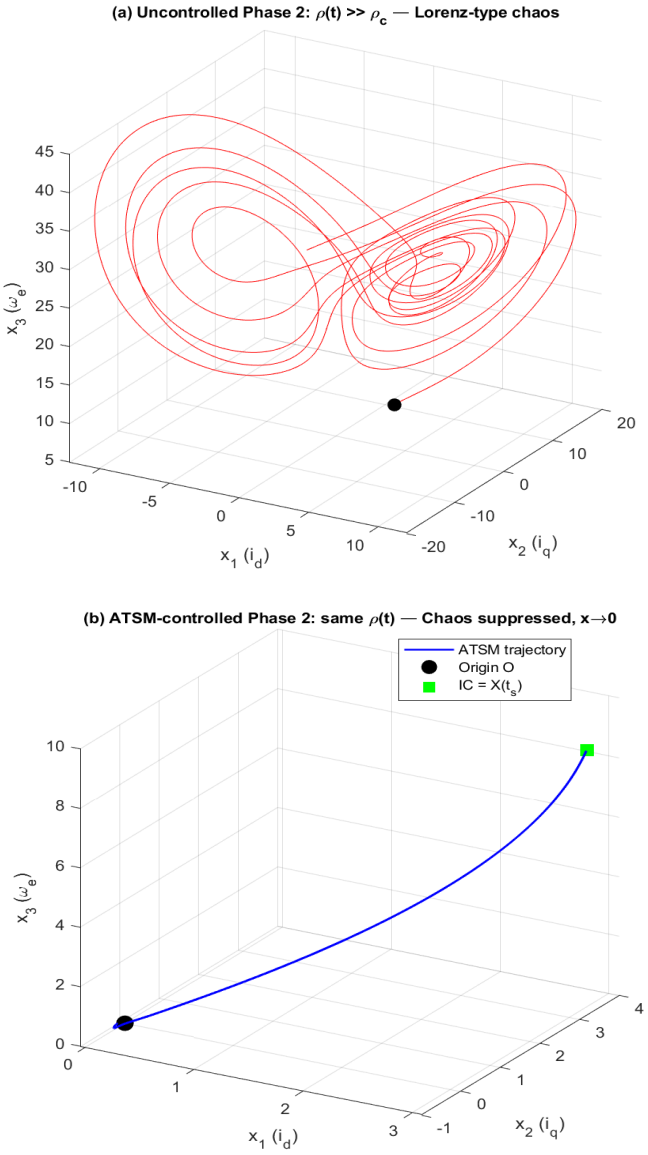

Figure 1. 3D phase portraits in Phase 2

(a) uncontrolled butterfly attractor; (b) ATSM controlled trajectory converging to origin

In Figure 1a, the uncontrolled trajectory forms a butterfly-shaped Lorenz attractor with $\max \| x \| = 45.39$, confirming chaos. In Figure 1b, ATSM drives the same trajectory to Oin finite time, with $t_{\text{conv}} = 0.818$s, confirming stabilization.

Figure 2 shows x_1, $x_2 = i_q$, $x_3 = i_d$ in Phase 2 for chaos (red) and ATSM (blue). Under ATSM, $x(t) \to 0$ within $t < 1$ s and $s_i \to 0$ with no visible chattering, consistent with the boundary layer $\text{sat}(s_i/\phi_{bl})$ smoothing. Over $t \in [0,30]$ s, Phase 1 with $t < t_s = 10$s and $\rho_1 = 10 < \rho_c = 14.93$ gives identical responses converging to $C^+ = [3,3,9]^T$with $\| x(t_s) - C^+ \| = 0.211$. For $t \geq t_s$, $\rho(t) > \rho_c \Rightarrow \lambda_{\max} > 0$ and the uncontrolled system becomes chaotic, while ATSM enforces $x(t) \to O$ and $\lambda_{\max} < 0$. This confirms the detection and trigger mechanism when $\rho(t)$ crosses the threshold in (10).

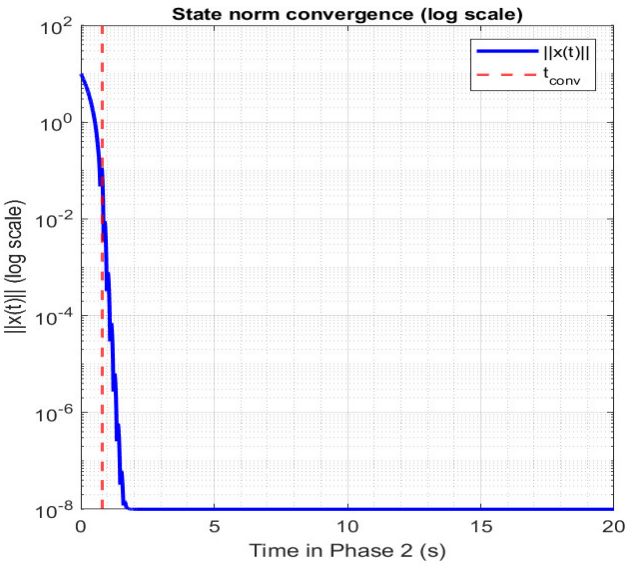

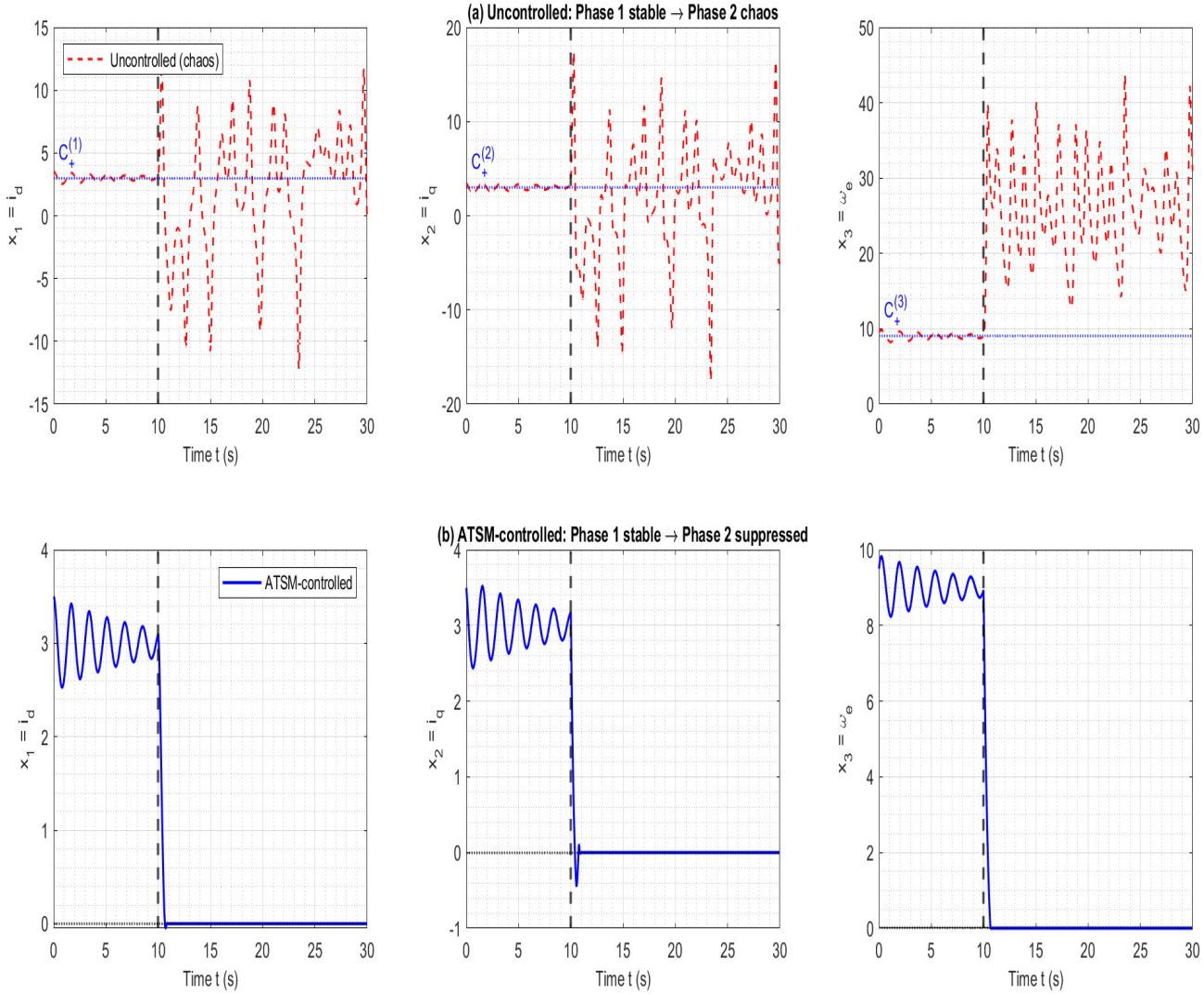

Figure 2. Two phase scenario: uncontrolled case and ATSM controlled case

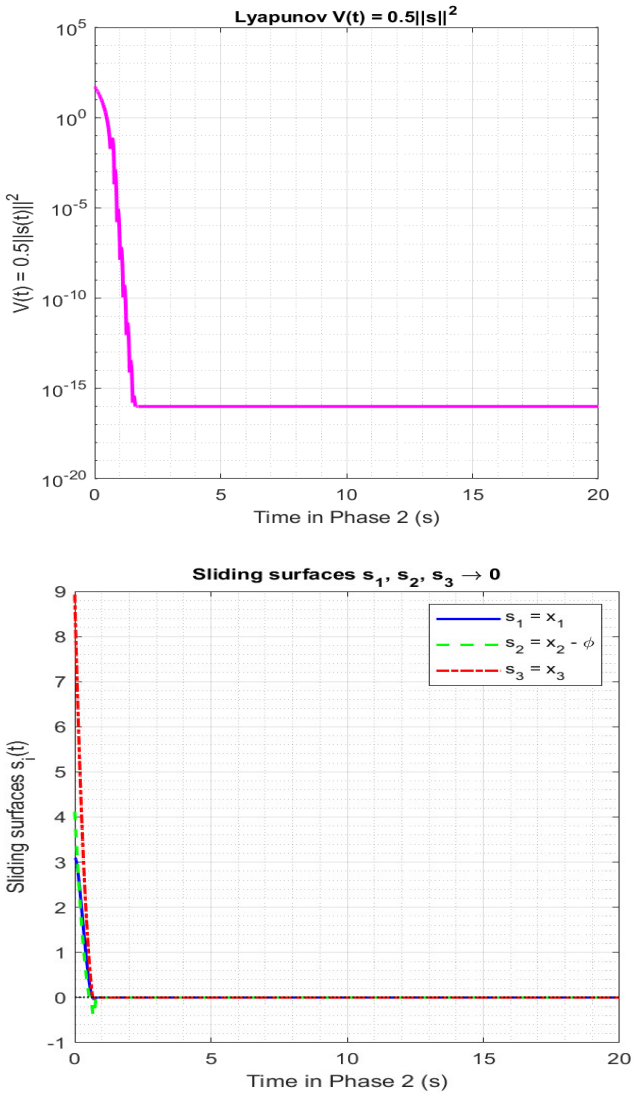

Figure 3. Finite-time convergence, Lyapunov decay, and sliding-surface evolution

Figure 3 demonstrates finite-time convergence of ATSM through three consistent arguments. In Figure 3a, the state norm satisfies $\| x(t) \| \to 0$ at $t_{conv} = 0.818$s, which is strictly smaller than the theoretical bound $t_{bound} = 3.211$s derived from the inequality $\dot{V} \leq -cV^{\alpha}$ with $0 < \alpha < 1 \Rightarrow t_{conv} \leq \frac{V(0)^{1-\alpha}}{c(1-\alpha)}$, confirming that the closed-loop system reaches the origin in finite time rather than asymptotically. In Figure 3b, the Lyapunov function $V(t) = \frac{1}{2} \| s(t) \|^2$ decreases from 53.15 to 3.03×10^{-320}, showing strict energy dissipation $V(t) \downarrow 0$; the few samples with $\dot{V} > 0$ appear only when $V \approx 10^{-320}$, i.e. at machine precision limit of float64, hence they are numerical artifacts and do not violate the theoretical condition $\dot{V} < 0$. In Figure 3c, the sliding variables $s_1 = x_1$, $s_2 = x_2 - \phi$, $s_3 = x_3$ converge to zero, that is $s(t) \to 0 \Rightarrow x(t) \to 0$, which ensures that the system trajectory is driven onto the sliding manifold and then to the equilibrium. Together, these results verify finite-time stability with both theoretical guarantee and numerical consistency.

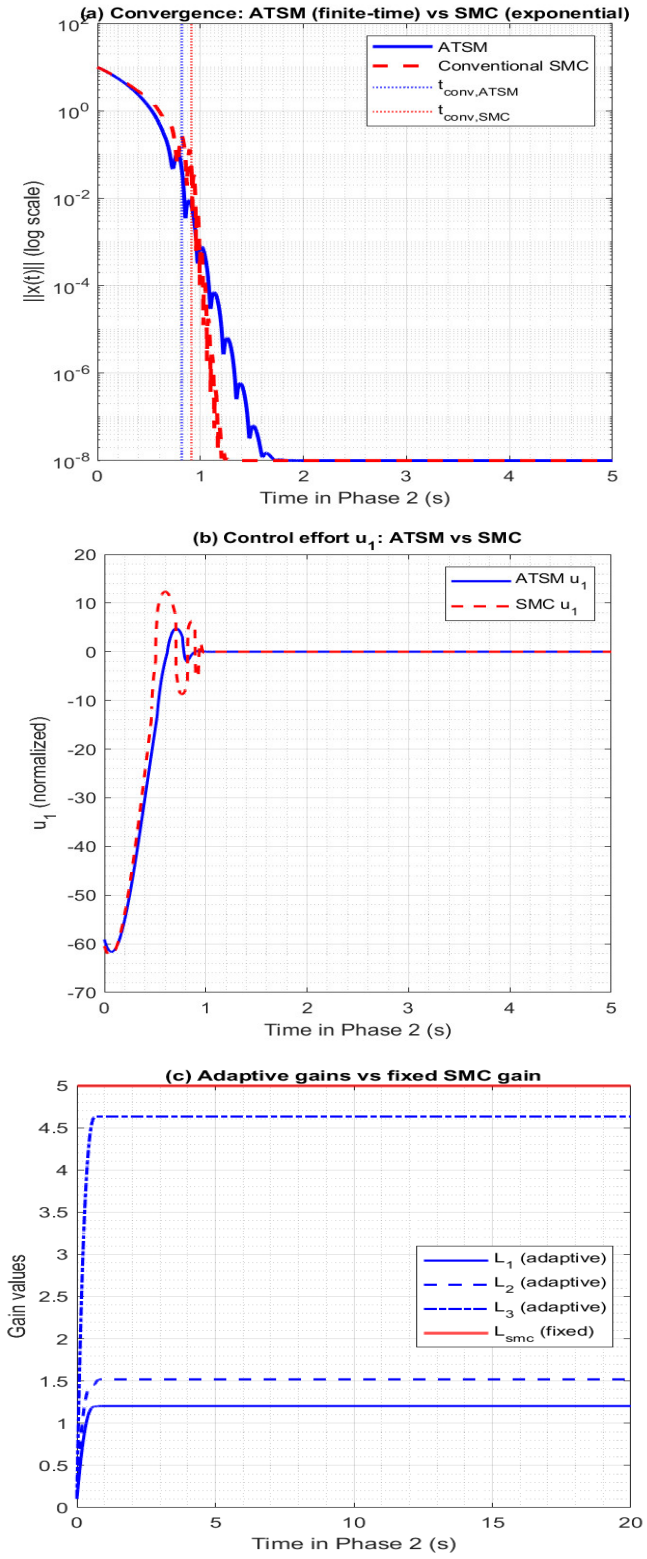

Figure 4. Comparison between ATSM and fixed-gain SMC

Figure 4 compares ATSM with fixed-gain SMC using the same sliding surface, but SMC removes $|\ s\ |^q$and sets $L_{\text{fixed}} = [5,5,5]$. ATSM reaches $t_{\text{conv}} = 0.818$s, while SMC reaches 0.913s, so ATSM is about 12% faster; ATSM also reduces ISE from 16.49 to 15.35 and mean gain from 5.0 to 2.45, i.e. about 7% and 51%. Finite-time convergence is consistent with the Bhat-Bernstein framework, whereas classical linear SMC is typically asymptotic convergence.

Table 1 summarizes the full set of quantitative results. In terms of convergence quality, ATSM reaches a final state norm of $\| x(T) \| = 4.7 \times 10^{-16}$ ⁰, which is effectively exact numerical zero, whereas SMC only reaches approximately 10^{-5} after 20s, consistent with asymptotic rather than finite-time behavior. Under a $\pm 10\%$ perturbation of the three parameters $(\sigma, \beta, \rho_{\text{amp}})$, the largest convergence time among all six test cases is 0.843s, which remains far below the 20 sduration of Phase 2. This indicates that the controller is not sensitive to moderate modeling errors.

Table 1. Quantitative performance comparison between ATSM and fixed-gain SMC

Metric	ATSM	Fixed-gain SMC
t_{conv}(s)	0.818	0.913
$\text{ISE} = \int \| x \|^2 \, dt$	15.35	16.49
Mean gain $(\bar{L})$	2.45	5.00
$\| x(T = 30\,\text{s}) \|$	4.7×10^{-16} ⁰	$\approx 10^{-5}$
ISE of u_1	1.172×10^3	1.121×10^3
ISE of u_2	1.183×10^2	9.458×10^1

4. CONCLUSION

This work establishes the chaos-detection condition of the PMLSM directly from the motor parameters through the Hopf structure of the Lorenz-equivalent model, leading to the feasibility condition $\sigma > \beta + 1$ and the critical threshold $\rho_c = \sigma(\sigma + \beta + 3)/(\sigma - \beta - 1)$. Under the two-phase scheduling $\rho_1 < \rho_c$ for $t < t_s$ and $\rho(t) > \rho_c$ for $t \geq t_s$, the system undergoes the transition $\mathcal{R}_{\text{st}} \to \mathcal{R}_{\text{ch}}$, i.e., $x(t) \to C^+$ before switching and $x(t) \in \mathcal{A}_{\text{L}}$ after switching, where $\mathcal{A}_{\text{L}}$ denotes a Lorenz-type chaotic attractor. Hence, chaos onset is characterized analytically by the sign change of $\rho(t) - \rho_c$, rather than inferred from trajectories alone.

The ATSM law combines the cascade sliding variables $s_1 = x_1$, $s_2 = x_2 - \phi$, $s_3 = x_3$ a feedback-linearized terminal structure, and the dead-zone adaptation $\dot{L}_i = \lambda_i \max\{|\ s_i\ | - d_z, 0\}$. With the augmented Lyapunov function $V = \frac{1}{2}\sum_{i=1}^{3} s_i^2 + \frac{1}{2}\sum_{i=1}^{3} \tilde{L}_i^2 / \lambda_i$, the closed-loop system satisfies $\dot{V} \leq -c_{\min}(2V)^{(1+q)/2}$, $0 < q < 1$, which implies $t_{\text{conv}} - t_s \leq \| s(t_s^+) \|_2^{1-q} / [c_{\min}(1-q)] < \infty$. Therefore, the closed-loop response satisfies $x(t) \to 0$in finite time, $\| x(T) \|_2 \to 0$, and $V(T) \ll V(0)$, so the stabilization mechanism is genuinely finite-time rather than asymptotic.

Quantitatively, the ATSM performance can be summarized by three relations: $|d(t)| \leq D$, $D \notin \mathcal{D}_{\text{design}} \Rightarrow x(t) \to \mathcal{B}_\varepsilon(0)$ with $\varepsilon \ll \sup_{\mathcal{A}_L} |x|2)$; $(p = (\sigma, \beta, \rho\text{amp})$, $\Delta p/p \in [-\delta, \delta] \Rightarrow t_{\text{conv}}(p) < \infty$, $\forall p \in \mathcal{P}_\delta$ with weak dispersion of $t_{\text{conv}}(p)$ and $\bar{L}_{\text{ATSM}} < L_{\text{SMC}}$, $t_{\text{conv}}^{\text{ATSM}} < t_{\text{conv}}^{\text{SMC}}$, $\text{ISE}_{\text{ATSM}} < \text{ISE}_{\text{SMC}}$. In compact form, the ATSM envelope is finite-time chaos suppression and robustness to bounded unknown disturbances and reduced gain demand with improved tracking quality.

Building on these findings, future work should focus on experimental validation on a real PMLSM platform, extension to unmatched disturbances via a sliding mode observer or EID estimation, online adaptation of σ and β under temperature-dependent parameter variations, and generalization to multi-axis PMLSM systems with coupled-axis chaotic dynamics requiring distributed or coordinated control.

ACKNOWLEDGMENT

The authors gratefully acknowledge Thai Nguyen University of Technology, Vietnam, for its support of this work.

REFERENCES

[1]. Zhao L., Luo S., Hu X., Ma H., Zhang J., "Accelerated adaptive backstepping control of the chaotic PMSM via the type-2 sequential fuzzy neural network," in *Proceedings of International Symposium on Autonomous Systems (ISAS)*, Guangzhou, China, 35-40, 2020.

[2]. De La Cruz N., Basin M., "Predefined-time control of full-scale 4D permanent-magnet synchronous motor," in *Proceedings of IEEE Conference on Systems, Process and Control (ICSPC)*, Malacca, Malaysia, 81-85, 2021.

[3]. Yin X., She J., Liu Z., Wu M., Kaynak O., "Chaos suppression in speed control for permanent-magnet synchronous motor drive system," *Journal of the Franklin Institute*, 357/18, 13283–13303, 2020.

[4]. Li K., Ding J., Sun X., Tian X., "Overview of sliding mode control technology for permanent magnet synchronous motor system," *IEEE Access*, 12, 71685-71704, 2024.

[5]. Zhang K., Wang L., Fang X., "High-order fast nonsingular terminal sliding mode control of permanent magnet linear motor based on double

disturbance observer," *IEEE Transactions on Industry Applications,* 58/3, 3696-3705, 2022.

[6]. Ding H., Zou X., Li J., "Sensorless control strategy of permanent magnet synchronous motor based on fuzzy sliding mode observer," *IEEE Access*, 10, 36743–36752, 2022.

[7]. Thanh N.B., Tuan N.N., Ha N.T., Chien V.V., "Sliding mode controller based on fuzzy logic for PMSM servo system with uncertain disturbance," *HaUI Journal of Science and Technology,* 59/1, 2023.

[8]. Dan H.N., Thang N.T., Thinh L.D., Ha V.T., Lam N.T., "Speed sensorless control of permanent magnet synchronous motors using sliding-mode observer," *HaUI Journal of Science and Technology,* 59/2A, 2023.

[9]. Zhang J., Yu H., Che Z., Pang Y., Zhong W., Zhang H., "Linear Hall sensors-based sliding mode control for permanent magnet linear synchronous motor drive systems," in *Proceedings of Asia Power and Electrical Technology Conference (APET),* Shanghai, China, 56-60, 2022.

[10]. Wang X., Dong Z., Qu C., Wang N., Li Y., Wang H., "Second-order nonsingular terminal sliding mode control of permanent magnet linear synchronous motor based on robust compensator," in *Proceedings of IEEE IECON*, Singapore, 1-6, 2023.

[11]. Wang X., Dong Z., Wang N., "Adaptive integral-type second-order nonsingular terminal sliding mode control of permanent magnet linear synchronous motor," in *Proceedings of IEEE Transportation Electrification Conference (ITEC Asia-Pacific),* Chiang Mai, Thailand, 1-6, 2023.

[12]. Zhao X.M., Gong Y.W., Jin H.Y., Xu C., "Adaptive super-twisting-based nonsingular fast terminal sliding mode control of permanent magnet linear synchronous motor," *Transactions of the Institute of Measurement and Control*, 2023.

[13]. Zhao X., Wang L., "Finite-time control of permanent magnet linear synchronous motor via variable gain fractional-order terminal sliding mode control," *IEEE Transactions on Transportation Electrification,* 11/4, 9105–9120, 2025.

[14]. Chen L., Zhang H., Wang H., Shao K., Wang G., Yazdani A., "Continuous adaptive fast terminal sliding mode-based speed regulation control of PMSM drive via improved super-twisting observer," *IEEE Transactions on Industrial Electronics*, 71/5, 5105–5115, 2024.

[15]. Wang L., Zhao J., Song J., Yu Z., Pan Z., "Model-free sliding mode control of permanent magnet linear synchronous motor using dynamic gain time delay estimation," *IEEE Transactions on Power Electronics,* 40/9, 12215-12229, 2025.

[16]. Phan D.H., Nguyen V.T., Bui T.L., Nguyen D.T., "Adaptive sliding mode control for twin rotor MIMO system using radial basis function neural network," *HaUI Journal of Science and Technology,* 61/7E, 2025.

[17]. Karimi A., Akbari H., Mousavi S., Beheshtipour Z., "Design of an adaptive terminal sliding mode to control the PMSM chaos phenomenon," *Systems Science & Control Engineering,* 11/1, 2023.